

HIGH- J $V=0$ SIS MASER EMISSION IN IRC+10216: A NEW CASE OF INFRARED OVERLAPS

J. P. FONFRÍA EXPÓSITO, M. AGÚNDEZ, B. TERCERO, J. R. PARDO AND J. CERNICHARO

Dept. Molecular and Infrared Astrophysics, Instituto de Estructura de la Materia, CSIC, C/ Serrano 121, 28006, Madrid (Spain)

Draft version October 25, 2018

Abstract

We report on the first detection of maser emission in the $J=11-10$, $J=14-13$ and $J=15-14$ transitions of the $v=0$ vibrational state of SiS toward the C-rich star IRC+10216. These masers seem to be produced in the very inhomogeneous region between the star and the inner dust formation zone, placed at $\simeq 5-7 R_*$, with expansion velocities below 10 km s^{-1} . We interpret the pumping mechanism as due to overlaps between $v=1-0$ ro-vibrational lines of SiS and mid-IR lines of C_2H_2 , HCN and their ^{13}C isotopologues. The large number of overlaps found suggests the existence of strong masers for high- J $v=0$ and $v=1$ SiS transitions, located in the submillimeter range. In addition, it could be possible to find several rotational lines of the SiS isotopologues displaying maser emission.

Subject headings: circumstellar matter — masers — stars: AGB and post-AGB — stars: carbon

1. INTRODUCTION

The detection of strong maser emission at the frequencies of pure rotational transitions of some molecules is a common phenomenon in circumstellar envelopes (CSE's) of evolved stars (Elitzur 1992; Gray 1999). The maser is usually produced in a small region of the envelope and sometimes provides valuable information on the physical conditions of the emitting region.

Due to the different chemistry, masers are produced by different molecules in O- and C-rich stars. In O-rich stars, SiO exhibits strong maser emission in different rotational transitions within several vibrational states, from $v=1$ to 4 (Cernicharo et al. 1993; Pardo et al. 1998). These masers are formed in a region of the CSE very close to the stellar surface and seem to be driven by NIR radiation (Pardo et al. 2004). In C-rich stars, although SiO is present with similar abundances than in O-rich stars (Schöier et al. 2006), no SiO maser has been detected. The explanation could be that SiO is formed at $\simeq 3-5 R_*$, where the angular dilution of the star is high and the density and temperature lower than in the regions where SiO masers are produced in O-rich stars (Agúndez & Cernicharo 2006). In C-rich stars only HCN shows strong maser emission in several pure rotational lines within vibrational states from $\nu_2=1$ to 4 (Lucas & Cernicharo 1989; Schilke & Menten 2003). These masers must be formed in the innermost regions of the CSE. SiS has been previously found to show weak maser emission in the $J=1-0$ $v=0$ transition in IRC+10216 (Henkel et al. 1983).

In this letter, we report on the first detection of maser emission from the $J=11-10$, $14-13$ and $15-14$ transitions in the $v=0$ vibrational state of SiS (hereafter M_1 , M_2 , and M_3) observed toward the C-rich star IRC+10216. We have also obtained observations of $v=1$ rotational lines which exhibit thermal emission. We propose that overlaps of $v=1-0$ ro-vibrational transitions of SiS with mid-IR lines of C_2H_2 and HCN could provide the pumping mechanism for these masers as well as higher- J $v=0$ SiS masers in the submillimeter range. This discovery is interesting because this species could play in C-rich stars a role similar to that of SiO in O-rich stars: the energy level pattern of both molecules is similar and it is also formed

close to the star, as chemical equilibrium and interferometric observations imply (Bieging & Nguyen-Q-Rieu 1989).

2. OBSERVATIONS

The observations of the $v=0$ $J=6-5$ and $J=8-7$ to $J=15-14$ transitions of SiS (see left panels, Fig. 1) were carried out on 2004 June 19th with the IRAM 30 m radio telescope. Four SIS receivers operating at 1, 1.3, 2, and 3 mm were used simultaneously. System temperatures were in the range 120-225 K for the 1, 1.3 and 2 mm receivers and 200-600 K for the 3 mm receivers. Atmospheric opacities ranged between 0.08 at 108 GHz to 0.28 at 267 GHz. For the $J=10-9$ SiS line at 181.5 GHz, the system temperature was significantly higher, $\simeq 10^4$ K, due to proximity to the atmospheric water line at 183.3 GHz. The intensity scale was calibrated using two absorbers at different temperatures according to the Atmosphere Transmission Model ATM (Cernicharo 1985; Pardo et al. 2001). Pointing and focus were regularly checked on the nearby quasar OJ 287. The observations were made in wobbling mode, with 180" offset and the secondary nutating at a rate of 0.5 Hz. The backends were a filter bank with 256 MHz bandwidth and 1 MHz resolution and an autocorrelator with 80 kHz resolution ($\Delta v \simeq 0.08-0.2 \text{ km s}^{-1}$). The lines of SiS in the $v=1$ state (see right panel, Fig. 1) were also observed with the IRAM 30 m telescope between 1989 and 2001.

Additionally we show some spectra corresponding to ro-vibrational lines of SiS (see center panels in Fig. 1) from a mid-IR high resolution spectrum (11-14 μm) obtained in 2002 December with the TEXES spectrometer mounted on the 3 m telescope IRTF (observational procedures described in Lacy et al. 2002; Fonfría Expósito et al. 2006).

3. RESULTS AND DISCUSSION

The $v=1$ rotational lines show single cusped profiles and their relative intensities indicate that the rotational levels are thermally populated. The linewidths correspond to velocities of $9-11 \text{ km s}^{-1}$, lower than the terminal velocity $\simeq 14.5 \text{ km s}^{-1}$ (Cernicharo et al. 2000), thus the emission arises from the innermost region of the

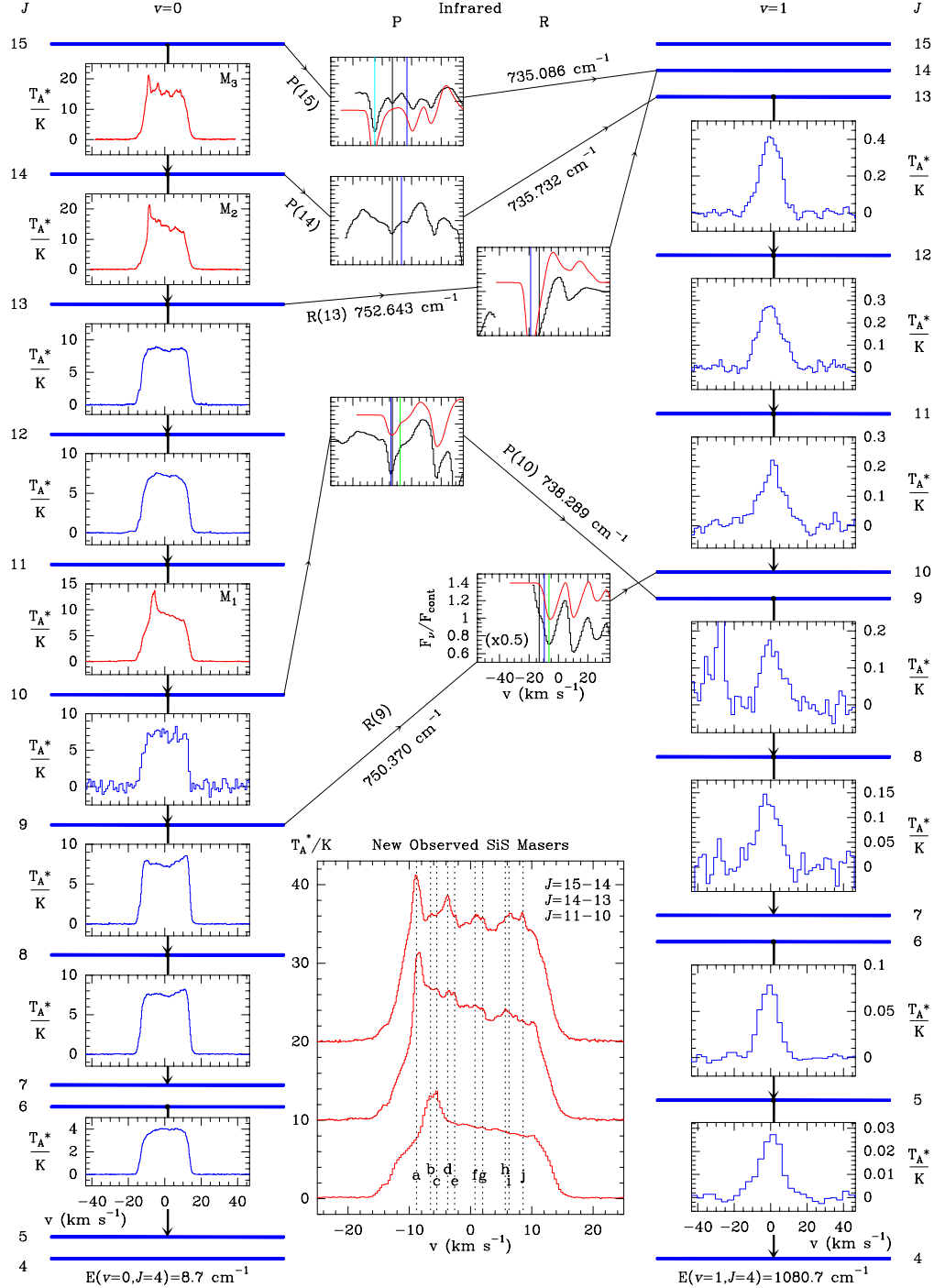


FIG. 1.— Millimeter and mid-IR observations towards IRC+10216. – The pure rotational transitions in the $v=0$ state (left inserts) and in the $v=1$ state (right inserts) are plotted as a function of the velocity with respect to the star ($v_{LSR} = -26.5$ km s $^{-1}$). The velocity structure of the three observed masers M_1 , M_2 and M_3 (plotted as red histograms) is shown in more detail in the middle-bottom insert, where the upper lines have been increasingly shifted by 10 K. – The middle inserts present some mid-IR spectra at the frequencies of several ro-vibrational $v=1-0$ SiS lines, whose labels and frequencies are also shown. The zero of the velocity scale is set to the SiS frequency corrected for the LSR. The observed spectrum is plotted as a black histogram. Red lines correspond to a radiative transfer model which only considers C_2H_2 , HCN and their isotopologues (Fonfría Expósito et al. 2006). The vertical lines indicate the position of maximum absorption for the transitions of SiS (black), C_2H_2 (dark blue), $H^{13}CCH$ (light blue) and HCN (green).

CSE, between the photosphere and the inner dust formation zone, placed at $\simeq 5 R_*$ (Keady et al. 1993). We can derive the SiS abundance in that region from the $v=1$ lines assuming an uniform sphere at a distance of 180 pc with a radius of $10 R_*$, illuminated by the central star ($R_*=5\times 10^{13}$ cm, $T_*=2300$ K), with $T_k=1000$ K and $n_{H_2}=1.6\times 10^9$ cm $^{-3}$ (mean values for this region derived by Fonfría Expósito et al. 2006) and an expansion velocity of 11 km s $^{-1}$. We solve the statistical equilibrium for SiS considering 100 rotational levels and 3 vibrational states and apply the LVG radiative transfer formalism using the code developed by J. Cernicharo. With the assumed n_{H_2} , the column density for H_2 is $\simeq 7\times 10^{23}$ cm $^{-2}$ and the derived one for SiS is $\simeq 5.0\times 10^{18}$ cm $^{-2}$. Hence, the SiS abundance is $\simeq 7\times 10^{-6}$. This result is compatible with a higher SiS abundance in the innermost CSE (from LTE chemistry models, 3×10^{-5} , Agúndez & Cernicharo 2006) and an abundance further away of 6.5×10^{-7} according to observations of $v=0$ rotational lines over the outer CSE by Bieging & Nguyen-Q-Rieu (1989).

Most $v=0$ rotational lines show a rounded or slightly double peaked profile with the blue part absorbed by cold SiS through the envelope. However, M_1 , M_2 and M_3 show extra emission in the form of narrow peaks (FWHM=1-3 km s $^{-1}$). The velocities of these features, within the -10 to 10 km s $^{-1}$ range, indicate that SiS maser emission arises from different regions located between the star and the inner dust formation zone ($r\simeq 5 R_*$). The lines M_2 and M_3 have been previously observed by Sahai et al. (1984) but no maser emission was noticed. This could be due either to the limited sensitivity of their observations or to a time variability of the SiS maser phenomenon. The bottom-center panel of Fig. 1 shows in detail the line profiles of the observed masers. Up to ten maser features labelled (a, \dots, j) are identified. The most complex line profile is that of M_3 . It is formed by 5 main features: a , d , f , i , j with $v=-8.8$, -3.7 , 0.88 , 6.3 and 8.4 km s $^{-1}$, respectively. The line profiles show that the strongest peaks are at negative velocities, having their red counterparts rather weak. This behavior was previously found by Henkel et al. (1983) for the $v=0$ $J=1-0$ line, which mostly consists of a narrow peak (FWHM=0.3 km s $^{-1}$) centered at -13.5 km s $^{-1}$. The strong asymmetry of the lineshapes can be either due to blanking by the star of the redshifted maser or by amplification of the blueshifted emission by the foreground stellar environment.

The strongest observed maser, M_3 , with $T_{MB}\simeq 60$ K ($F_{obs}\simeq 300$ Jy; with thermal and non-thermal emission), is weak compared to some SiO masers detected in O-rich stars (e.g. Cernicharo et al. 1993) or to HCN masers observed in IRC+10216 (Lucas & Cernicharo 1989; Schilke & Menten 2003). However, M_1 , M_2 , and M_3 are stronger than the SiS $J=1-0$ maser observed towards IRC+10216 by Henkel et al. (1983). The similarity between maser features in M_2 and M_3 indicates that they may arise from the same regions and produced by the same pumping mechanism; the maser in M_1 is probably formed in other regions. Hence, we suggest two possible geometries of the innermost CSE to explain the observed features:

(i) An onion-like innermost region, where each maser is produced in a shell. This hypothesis is supported by the symmetry of features $a-j$ and $d-i$. The peaks at extreme

velocities, a and j , would be produced just in front of and behind the star near the inner dust formation shell ($r\simeq 5 R_*$) with expansion velocities of $\simeq 5-11$ km s $^{-1}$. The features d and i would be produced in a similar way but in an inner shell with a lower expansion velocity. Finally, the central peak, f , would be formed in a shell very close to the star, with the whole shell contributing to the maser emission. M_1 would be produced in a cap-shaped region in front of the star.

(ii) All the masers are formed in different positions of a clumpy shell. The different features in M_2 and M_3 would be produced in different regions of the shell: peaks a and j in front of and behind the star and the other peaks (d , f , and i) in different clumps, as occur with the only feature of M_1 .

The classic pumping mechanism for the SiO $v>0$ masers observed in O-rich stars resides in the increase of the trapping lifetime $(A/\tau)_{v\rightarrow v-1}$ with J for $v\rightarrow v-1$ transitions, when they become optically thick (Kwan & Scoville 1974). Such mechanism produces masers in adjacent rotational lines of the v state, and explains the $v=1$ and 2 SiO masers (Bujarrabal & Nguyen-Q-Rieu 1981; Lockett & Elitzur 1992). However, the masers observed in rotational transitions of ^{29}SiO , ^{30}SiO , and in $v=3$ and 4 of SiO do not show the latter behavior and have been interpreted as due to IR overlaps between ro-vibrational lines of SiO isotopologues (Cernicharo et al. 1991; González-Alfonso & Cernicharo 1997). For SiS, the absence of maser emission in $v=1$ rotational lines and the odd $v=0$ pattern also exclude the Kwan & Scoville pumping mechanism. This suggests that overlaps of $v=1-0$ ro-vibrational transitions of SiS with those of mode ν_5 of C_2H_2 and mode ν_2 of HCN, could provide the pumping mechanism. C_2H_2 and HCN are abundant in the inner CSE of IRC+10216 and dominate the 11-14 μm spectrum (Fonfría Expósito et al. 2006). Overlaps with these two species have been already proposed by Sahai et al. (1984) to explain the different profiles of adjacent J lines of SiS. However, the SiS frequencies used in that work were not as accurate ($\sigma\sim 10^{-1}$ cm $^{-1}$) as those available today. We have calculated those frequencies from the Dunham coefficients determined by Sanz et al. (2003), for which the error of the band center is $<10^{-4}$ cm $^{-1}$ ($\simeq 0.04$ km s $^{-1}$; the relative accuracy of P and R lines is much better). The frequencies of C_2H_2 , H^{13}CCH , HCN, and H^{13}CN lines have been taken from the HITRAN Database 2004 (Rothman et al. 2005), with an accuracy better than 10^{-3} cm $^{-1}$ ($\simeq 0.4$ km s $^{-1}$) for C_2H_2 and H^{13}CCH , and 10^{-4} cm $^{-1}$ for HCN and H^{13}CN .

Table 1 shows the mid-IR line overlaps of SiS with C_2H_2 , HCN, and their most abundant isotopologues. For the overlap search we selected coincidences within $|\Delta v|<10$ km s $^{-1}$. However, since the CSE is expanding, every region of the envelope is receding from the others. Hence, if the population of the SiS levels is affected by an overlap with a strong line of other species, the frequency of this overlapping transition must be higher than the SiS one. This would restrict the condition to positive Δv . Nevertheless, due to the linewidth, lines at $\Delta v<0$ can overlap the SiS lines. Hence, we have set the negative cutoff to one half of the typical linewidth in the innermost CSE ($\simeq 5$ km s $^{-1}$; Fonfría Expósito et al. 2006). There-

TABLE 1
MID-INFRARED LINE OVERLAPS OF SiS WITH C₂H₂, HCN, AND
THEIR MOST ABUNDANT ISOTOPOLOGUES

| Line | ν (cm ⁻¹) | Mol. | Transition | Δv (km/s) |
|----------------------------------------------------------|---------------------------|-------------------------------|-------------------------------------------------------------------------------------|-------------------|
| Overlaps Involving SiS Levels of Observed Lines | | | | |
| R 9 | 750.3695 | HCN | 01 ¹ 0 – 00 ⁰ 0 R _e (12) | -6.6 |
| P10 | 738.2889 | C ₂ H ₂ | 1 ⁻¹ 1 ¹ – 1 ⁻¹ 0 ⁰ R _f (3) | 1.2 |
| R13 | 752.6431 | C ₂ H ₂ | 0 ⁰ 1 ¹ – 0 ⁰ 0 ⁰ R _e (9) | 5.9 |
| P14 | 735.7324 | C ₂ H ₂ | 0 ⁰ 1 ⁻¹ – 0 ⁰ 0 ⁰ Q _e (38) | -6.1 |
| P15 | 735.0861 | C ₂ H ₂ | 0 ⁰ 1 ⁻¹ – 0 ⁰ 0 ⁰ Q _e (36) | -9.9 |
| Overlaps Involving SiS Levels of Unobserved Lines | | | | |
| P 2 | 743.2624 | C ₂ H ₂ | 0 ⁰ 1 ¹ – 0 ⁰ 0 ⁰ R _e (5) | 0.6 |
| P16 | 734.4368 | C ₂ H ₂ | 0 ⁰ 1 ⁻¹ – 0 ⁰ 0 ⁰ Q _e (34) | 1.1 |
| P20 | 731.8114 | C ₂ H ₂ | 0 ⁰ 1 ⁻¹ – 0 ⁰ 0 ⁰ Q _e (24) | 9.5 |
| P22 | 730.4815 | C ₂ H ₂ | 1 ⁻¹ 1 ¹ – 1 ¹ 0 ⁰ Q _e (18) | -2.1 |
| R22 | 757.5819 | C ₂ H ₂ | 1 ¹ 1 ¹ – 1 ¹ 0 ⁰ R _e (10) | 0.1 |
| R22 | 757.5819 | H ¹³ CN | 01 ¹ 0 – 00 ⁰ 0 R _e (17) | 5.2 |
| P23 | 729.8123 | H ¹³ CCH | 0 ⁰ 1 ⁻¹ – 0 ⁰ 0 ⁰ Q _e (19) | 8.7 |
| P24 | 729.1402 | C ₂ H ₂ | 0 ⁰ 1 ⁻¹ – 0 ⁰ 0 ⁰ Q _e (1) | 9.4 |
| P25 | 728.4654 | H ¹³ CCH | 0 ⁰ 1 ⁻¹ – 0 ⁰ 0 ⁰ Q _e (7) | -0.0 |
| R25 | 759.1733 | HCN | 01 ¹ 0 – 00 ⁰ 0 R _e (15) | 3.6 |
| R26 | 759.6977 | C ₂ H ₂ | 0 ⁰ 1 ¹ – 0 ⁰ 0 ⁰ R _e (12) | -1.0 |
| R33 | 763.2816 | H ¹³ CN | 01 ¹ 0 – 00 ⁰ 0 R _e (19) | 6.1 |
| P38 | 719.4363 | C ₂ H ₂ | 1 ¹ 1 ¹ – 1 ¹ 0 ⁰ P _e (5) | 4.5 |
| R40 | 766.7130 | C ₂ H ₂ | 0 ⁰ 1 ¹ – 0 ⁰ 0 ⁰ R _e (15) | 4.3 |
| R42 | 767.6652 | C ₂ H ₂ | 1 ¹ 1 ⁻¹ – 1 ¹ 0 ⁰ R _e (20) | 8.7 |
| R45 | 769.0697 | C ₂ H ₂ | 0 ⁰ 1 ¹ – 0 ⁰ 0 ⁰ R _e (16) | -1.8 |
| P48 | 712.1720 | C ₂ H ₂ | 1 ⁻¹ 1 ⁻¹ – 1 ⁻¹ 0 ⁰ P _f (8) | 4.7 |

NOTE. — Overlaps of SiS with C₂H₂, H¹³CCH, HCN and H¹³CN found in the mid-IR range [690, 780] cm⁻¹ with $-2.5 \leq \Delta v \leq 10$ km s⁻¹, where $\Delta v/c = [\nu(X) - \nu(\text{SiS})]/\nu(\text{SiS})$ and $J \leq 50$, (corresponding SiS $v=0$ rotational frequencies below 900 GHz). The lines and frequencies at the left correspond to the vibrational transitions $v=1 \rightarrow 0$ of SiS. The errors on the velocities are < 0.5 km s⁻¹. The notation for the C₂H₂ and H¹³CCH vibrational states involved in the ro-vibrational transitions is $\nu_4^{\epsilon_4} \nu_5^{\epsilon_5}$, whereas for HCN and H¹³CN is $\nu_1 \nu_2 \nu_3$. The parity of the lower level is even (e) and odd (f). The transitions are labelled as R, P, and Q for $J_{up} - J_{low} = +1, -1, 0$.

fore, our search is restricted to $-2.5 \leq \Delta v \leq 10$ km s⁻¹. All the ro-vibrational SiS lines commented hereafter refer to $v=1 \rightarrow 0$ transitions and will be labelled with the usual spectroscopic nomenclature R, Q, P (see footnote of Table 1).

In order to qualitatively interpret the effects of IR overlaps on maser emission, we have used the same LVG radiative transfer code modified to account for overlaps, changing the intensity at the overlapping frequency and the escape probability for photons from the overlapped lines. Thus, for some SiS lines, the excitation temperature becomes negative (maser activation) and the brightness temperature is considerably enhanced. M₂ and M₃

are naturally explained by the overlap of the R(13) line of SiS with the strong C₂H₂ line 0⁰1¹ – 0⁰0⁰R_e (9) (Table 1). SiS molecules are easily excited from $v=0$ $J=13$ to $v=1$ $J=14$ through R(13) and decay to the $v=0$ $J=15$ via P(15), creating a population inversion between the $v=0$ $J=13$ and 15, and producing maser emission in M₂ and M₃. M₁ may be produced by the overlap of the P(10) SiS line with the strong C₂H₂ line 1⁻¹1¹ – 1⁻¹0⁰R_f (3). This overlap can pump SiS molecules from $v=0$ $J=10$ to $v=1$ $J=9$ through P(10), depopulates the $v=0$ $J=10$ level and produces the inversion between $v=0$ $J=10$ and 11.

We have also looked for overlaps of $v=1-0$ higher- J SiS lines with C₂H₂ and HCN transitions to try to predict SiS masers at submillimeter wavelengths. Some of them are shown in the second block of Table 1. They suggest, for example, that a maser could be found in rotational transitions involving the $v=0$ $J=23$ level (likely $J=24-23$ and maybe 23-22), or the $v=0$ $J=25$ and 26 states (perhaps in the $v=0$ $J=27-26$ and maybe 26-25). These overlaps could also produce masers in $v=1$ rotational transitions.

There are many overlaps of other SiS isotopologues with lines of C₂H₂, HCN and ²⁸Si³²S. With the adopted criteria for the overlap search (see footnote of Table 1), we have found 91, 93, 76, and 94 coincidences for ²⁹SiS, ³⁰SiS, Si³⁴S, and Si³³S, respectively. Consequently, although these species are less abundant than ²⁸Si³²S, the population of some levels could be inverted producing maser emission.

This study represents the discovery of three new SiS masers and should be complemented with future observations of higher- J $v=0$ and 1 rotational transitions. Furthermore, a detailed multi-molecule non-local radiative transfer model would help to understand the dust formation region and the role of SiS in C-rich evolved stars.

We want to thank the IRAM staff, M. J. Richter (NSF grant AST-0307497), J. H. Lacy (NSF grant AST-0205518), and collaborators for the mid-infrared observations, and Spanish MEC for funding support through grant ESP2004-665, AYA2003-2785, and “Comunidad de Madrid” Government under PRICIT project S-0505/ESP-0237 (ASTROCAM). This study is supported in part by the European Community’s human potential Programme under contract MCRTN-CT-2004-51230, Molecular Universe.

REFERENCES

- Agúndez, M. & Cernicharo, J., 2006, ApJ, astro-ph/0605645
 Bieging, J., H. & Nguyen-Q-Rieu, 1989, ApJ, 343, L25
 Bujarrabal, V. & Nguyen-Q-Rieu, 1981, A&A, 102, 65
 Cernicharo, J. 1985, ATM: A Program to Compute Atmospheric Opacity between 0 and 1000 GHz, IRAM Internal Report
 Cernicharo, J., Bujarrabal, V., & Lucas, R., 1991, A&A, 249, L27
 Cernicharo, J., Bujarrabal, V., & Santarén, J., L., 1993, ApJ, 407, L33
 Cernicharo, J., Guélin, M., & Kahane, C., 2000, A&AS, 142, 181
 Elitzur, M., 1992, ARA&A, 30, 75
 Fonfria Expósito, J. P., Cernicharo, J., Richter, M. J., & Lacy, J., 2006, ApJ, submitted
 González-Alfonso, E. & Cernicharo, J., A&A, 322, 938
 Gray, M., 1999, Philos. Trans. R. Soc. London A., 357, 3277
 Henkel, C., Matthews, H. E., & Morris, M., 1983, ApJ, 267, 184
 Keady, J. J., Hall, D. N. B., & Ridgway, S., T., 1988, ApJ, 326, 832
 Keady, J. J. & Ridgway, S., T., 1993, ApJ, 406, 199
 Kwan, J. & Scoville, N., 1974, ApJ, 194, L97
 Lacy, J. H., Richter, M. J., Greathouse, T. K. et al., 2002, PASP, 114, 153
 Lafont, S., Lucas, R., & Omont, A., 1982, A&A, 106, 201
 Lockett, P. & Elitzur, M., 1992, ApJ, 399, 704
 Lucas, R. & Cernicharo, J., 1989, A&A, 218, L20
 Pardo, J. R., Cernicharo, J., González-Alfonso, E., & Bujarrabal, V., 1998, 329, 219
 Pardo, J. R., Cernicharo, J., & Serabyn, G., 2001, IEEE Trans. Antennas Propagation, 46, 1683
 Pardo, J. R., Alcolea, J., Bujarrabal, V., Colomer, F., del Romero, A., & de Vicente, P., 2004, 424, 145

- Rothman, L. S., Jacquemart, D., et al., 2005, J. Quant. Spec. Radiat. Transf., 96, 139
- Sahai, R., Wootten, A., & Clegg, R. E. S., 1984, ApJ, 284, 144
- Sanz, M. E., McCarthy, M. C., & Thaddeus, P., 2003, J. Chem. Phys., 119, 11715
- Schilke, P. & Menten, K. M., 2003, ApJ, 583, 446
- Schöier, F. L., Olofsson, H., & Lundgren, A. A., 2006, A&A, astro-ph/0604213